Sensors and Actuators B 135 (2009) 618–624

Contents lists available at ScienceDirect

Sensors and Actuators B: Chemical

journal homepage: www.elsevier.com/locate/snb

Microfabricated electrochemical nitrate sensor using double-potential-step chronocoulometry

Dohyun Kim*, Ira B. Goldberg, Jack W. Judy

Electrical Engineering Department, University of California, Los Angeles, Los Angeles, CA 90095, United States

ARTICLE INFO

Article history:
Received 12 June 2008
Received in revised form 4 September 2008
Accepted 19 September 2008
Available online 1 October 2008

Keywords:
Electrochemical sensor
Chronocoulometry
Nitrate sensor
Microfabrication

ABSTRACT

A simple, miniaturized, and yet sensitive electrochemical nitrate sensor has been designed, fabricated and tested. The thin-film silver sensing electrode, silver-oxide reference electrode, and platinum counter electrode are microfabricated on a silicon substrate. A polyimide insulation layer is also patterned to improve reliability of a sensor chip. The sensor chip incorporates microfluidic channels. A fixture is also created to integrate the sensor chip and fluidic connectors for on-line flow-through analysis. The electrolyte is 0.01 M sodium hydroxide. The nitrate concentration is determined by double-potential-step chronocoulometry (DPSC) because it improves signal-to-noise ratio compared to amperometry and minimizes oxygen background current. Interference analysis of DPSC with 10 ions commonly found in groundwater indicates that HPO_4^{2-}/PO_4^{3-}, Ca^{2+}, and Sr^{2+} cause significant interference (i.e., more than 20% signal distortion). Performance characterization of sensor chips indicates that the limit of detection (LOD) and the upper limit of the linear range have a chip-to-chip variation of 4–75 μM and 500–2000 μM, respectively.

1. Introduction

The authors present a microfabricated nitrate sensor that uses double-potential-step chronocoulomtry (DPSC) to measure concentration. This study was undertaken to assess the feasibility of creating a simple and miniaturized nitrate sensor that is compatible with modern microfabrication techniques, and that has sufficient sensitivity and reliability for various applications. The ultimate goal of this work is to develop a new analytical tool that could be transformed into an inexpensive and mass-producible microsensor.

Excessive nitrate in drinking-water sources can present severe risks to human health, especially for infants [1]. Nitrate is easily converted to nitrite in the digestive systems of babies, and nitrite over a critical limit can cause *methemoglobin* that reduces the oxygen-carrying capacity of blood (i.e., blue-baby syndrome). Therefore, the U.S. Environmental Protection Agency (EPA) set the maximum contaminant level (MCL) for nitrate at 0.7 mM [2].

The interest in sensor networks has grown [3,4] because many believe they will become a very effective infrastructure for analyzing contamination information in real-time, over large areas, and without human intervention. A crucial step in realizing such sensor networks is the development of analytical systems that are sensitive enough for target applications, and more importantly, sufficiently reliable for unattended operation over long periods of time [4,5]. Also, such analytical systems need to be highly miniaturized and low cost for large-scale deployment and high-spatial-resolution sensing.

Nitrate determination has been a challenge to the field of analytical chemistry for a long time. Despite much published work on this topic, the *de facto* standard for nitrate detection continues to be spectrophotometry based on the Griess assay published in 1879 [6]. However, conventional bench-top techniques (e.g., UV/vis spectrometry, chromatography, and capillary electrophoresis) usually require expensive and large instruments, complex procedures, and multiple reagents. As a result, in practice, samples are manually taken from sources and brought to the laboratory for analysis. Therefore, these approaches are not suitable for low-cost, real-time applications.

Electrochemical methods can be a more viable approach for such applications because they are relatively simple and sufficiently sensitive. In particular, amperometric techniques have sufficient sensitivity, and low LOD (typically 0.1–10 μM) [6]. A broad linear range (2–4 orders of magnitude) is also readily obtainable [6]. In DPSC, an amperometric technique, current is integrated over a time period to increase the signal-to-noise ratio (SNR) and separate non-Faradaic components from the analytic signal [7]. Also, the potential steps used in the DPSC technique can separate oxygen background current from the analytical signal [8].

Silicon-based microfabrication is proven to be an efficient manufacturing technique for disposable chemical microsensors

* Corresponding author. Tel.: +1 310 206 3995; fax: +1 310 206 8495.
E-mail address: dohyun@ee.ucla.edu (D. Kim).

0925-4005/$ – see front matter © 2008 Elsevier B.V. All rights reserved.
doi:10.1016/j.snb.2008.09.022

with high-productivity, low-cost, and excellent manufacturing reproducibility [9]. Microfabrication also opens the possibility of integration of microelectronics, such as amplifiers, filters, a microprocessor, and a wireless radio to enable a smart sensor. Metal electrodes were studied in this work, rather than biologically or chemically modified electrodes or non-metal electrodes, to allow straightforward microfabrication.

The proposed microfabricated sensor uses a simple electrochemical system: silver sensing electrode, silver-oxide reference electrode, and platinum counter electrode in 0.01 M NaOH electrolyte. The microelectrodes and microfluidic channels are microfabricated on a silicon substrate. Nitrate concentration is detected using DPSC, in which current accruing from nitrate reduction to nitrite is integrated. The sensor is characterized for LOD, linear range, and linearity.

2. Experimental

2.1. Chemical reagents

All chemicals are American Chemical Society (ACS) Reagent grade. All solutions were prepared with 10 M Ω cm deionized water (Super-Q Plus, Millipore, Billerica, MA, USA). Sodium-hydroxide electrolytes were freshly prepared from pellets to minimize carbonate contamination. For the interference study, 1 M stock solutions of 10 different ionic species that are commonly found in groundwater were prepared from sodium salts ($NaNO_2$, NaCl, Na_3PO_4, Na_2SO_4, NaF, Na_2CO_3, and $NaBO_2 \cdot 4H_2O$) and acetate salts ($KC_2H_3O_2$, $Ca(C_2H_3O_2)_2 \cdot H_2O$, and $Sr(C_2H_3O_2)_2 \cdot xH_2O$).

2.2. Apparatus

Characterization of sensor chips was conducted with an electrochemical workstation (CHI-660B, CH Instrument, Austin, TX, USA) and a miniature Ag/AgCl reference electrode (RE-5B, Bioanalytical System, West Lafayette, IN, USA). All measurements were performed in a Faraday cage (CHI-200, CH Instrument, Austin, TX, USA).

2.3. Double-potential-step chronocoulometry (DPSC)

In DPSC, two potential steps are applied, and the resulting currents are numerically integrated and subtracted to measure the net nitrate reduction charge $Q_{NO_3^-}$. Two advantages of DPSC over current measurement are minimizing the oxygen background current and improving the SNR. Compared to the oxygen-free electrolyte, a significant increase in baseline current (i.e., $-0.16\,mA/cm^2$) was observed due to the reduction of dissolved oxygen ($O_2 + 2H_2O + 4e^- \rightarrow 4OH^-$) when the electrolyte was not purged with an inert gas [8]. The SNR is improved by integrating nitrate reduction current, because the Faradaic component of integration grows faster than the noise components. The detailed theoretical and experimental analysis of DPSC techniques is described elsewhere [8].

The complete experimental procedure of DPSC is as follows. (1) Nitrate and NaOH solution is prepared. (2) The sensing electrode is electrochemically activated. Activation consists of 10 potential scans between −1.2 and 1.0 V vs. Ag/AgCl reference electrode (unless otherwise stated) at a sweep rate of 1 V/s followed by 10 potential pulses between −0.25 and 0.9 V (0.5 s pulse-width). (3) The sensing electrode is biased at $E_1 = -0.5$ V from open-circuit potential (OCPT) for 4 s. Holding the electrode potential at E_1 for more than 2 s causes the oxygen-reduction current to reach a small steady-state level. After 3 s, the current is numerically integrated for 1 s, to calculate the oxygen reduction charge Q_1. (4) The potential is then stepped from E_1 to E_2 (−0.98 V), where is diffusion-controlled regime for nitrate and oxygen reduction. Therefore the nitrate reduction begins, and the oxygen-reduction current is still in a steady-state condition of the same magnitude as prior to E_2. The double-layer charging current, which is a non-Faradic component of the measured current, has subsided significantly at 40 ms after second potential step is applied. The oxygen- and nitrate-reduction currents are integrated for 1 s (i.e., nitrate- and oxygen-reduction charge, Q_2). (5) The net nitrate-reduction charge $Q_{NO_3^-}$ is then calculated by subtracting Q_1 from Q_2 (i.e., $Q_{NO_3^-} = Q_2 - Q_1$).

2.4. Sensor-chip fabrication

Sensor chips for nitrate determination were microfabricated in the UCLA Nanoelectronics Research Facility. Fig. 1 depicts a sensor chip and its principal components (i.e., microelectrodes, microfluidic channels, polyimide protection layer, electrical interconnects, and contacts). An SEM image (Fig. 1b) shows the shape and arrangement of microelectrodes and microfluidic channels. The sensor chips were microfabricated on a silicon substrate. The entire fabrication process is summarized in Fig. 2.

A silicon-oxide insulation layer was grown on the silicon wafer. An e-beam evaporator (Mark 40, CHA Industries, Fremont, CA, USA) was used to deposit platinum, and then silver layers. Titanium was used as the adhesion-layer material for both metals since a chromium adhesion layer severely corroded during the electrochemical activation process. The silver sensing and reference electrodes, and the platinum counter electrode were patterned

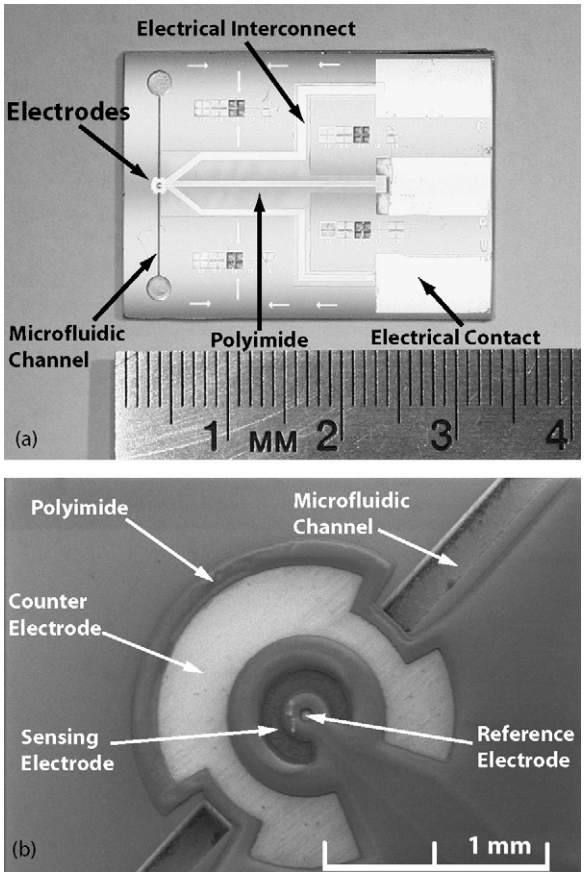

Fig. 1. (a) Photograph of a sensor chip (note: 1 mm = 1division) and (b) SEM image of its major components micromachined on a silicon substrate.

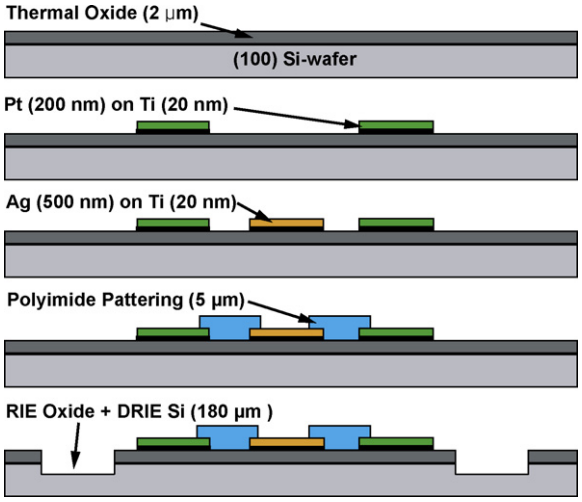

Fig. 2. Fabrication process for the sensor chip.

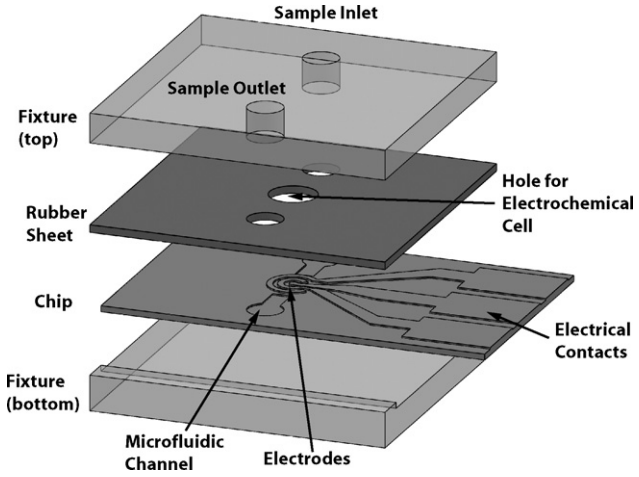

Fig. 3. Schematic of a fixture enclosing a sensor chip.

with a lift-off process. The electrical interconnects and contacts for the electrodes were also patterned on the same metal layers. The sensing and counter electrodes were designed to be concentric to improve the uniformity of the current distribution between the electrodes. The shape of sensing electrode is a 310° arc of a ring with an inner diameter of 65 μm and an outer diameter 175 μm. The geometric area of the sensing electrode is 0.710×10^{-3} cm^2. The counter electrode has also similar shape and its area is 7.7×10^{-3} cm^2, which is 10.8 times larger than the sensing electrode. The larger area of the counter electrode prevents oxygen-bubble formation on the counter electrode surface due to OH^- oxidation (i.e., $4OH^- \rightarrow 2H_2O + O_2 + 4e^-$) that occurs at a high current densities. The reference electrode is located close to the sensing electrode to minimize the uncompensated ohmic drop. As shown in Fig. 1b, the reference electrode is positioned at the center of the concentric electrodes. To simplify fabrication and prevent chloride contamination, Ag/AgCl was not used as an on-chip reference electrode. Instead, a silver electrode (1.96×10^{-5} cm^2) was used, since a sufficiently stable potential (i.e., 25 mV drift over 10 h) was observed for a 99.99% silver wire in 0.01 M NaOH electrolyte. However, thin-film silver was less stable than silver wire, even though it was deposited with a high-purity silver source. The reference potential of the thin-film silver electrode drifted too quickly to be used (i.e., 100 mV drift over minutes). The reason for such rapid drift is not understood at this time. To solve the potential-drift issue, silver was anodized at 0.4 V in 0.01 M NaOH for at least 17 min to form silver oxide, which showed greater stability (i.e., 50 mV drift over 2 h).

A polyimide passivation layer was patterned to improve the reliability of the sensor chips; a 5-μm-thick low-stress photodefinable polyimide (PI-2731, HD Microsystem, Parlin, NJ, USA) layer was deposited and hardened (i.e., spun on at 4000 rpm for 60 s, and cured at 350 °C for 1 h in a nitrogen-purged oven). Silver particles, that were formed on the sensing electrode during the electrochemical activation process, created a physical and electrical bridge to the reference electrode that resulted in a short-circuit when there was no polyimide layer. Consequently, erratic responses were observed. The 5-μm-tall polyimide wall, covering the circumference of the electrodes, prevented the reference-electrode short-circuiting problem. The polyimide layer also fully covered the electrical interconnects, and no electrolyte leakage was observed. A pair of 174-μm-wide, 180-μm-deep, and 8.3-mm-long microchannels were etched using deep reactive-ion etching (DRIE) after the silicon-oxide layer was patterned and etched.

2.5. A fixture for flow-through analysis

After the sensor chips were first characterized in a glass beaker containing the electrolyte, a special fixture (Fig. 3) was machined to make the measurement process quick and convenient. The overall size of the fixture including a chip is 3.8 cm × 3.8 cm × 2 cm. The fixture was machined at the UCLA School of Engineering and Applied Science R&D shop. The top and bottom portions of the fixture are made of Plexiglas. A rubber sheet (EPDM) is placed between the two Plexiglas plates, and has three punched holes: one for the microelectrochemical cell (volume ≃ 1.8 μl) and two for the through holes to the microfluidic channels. These holes are visually aligned with the sensor chip before assembling the fixture so that the circular fluidic inlet and outlet on the chip match the two through holes and electrodes are situated at the center of the middle hole (i.e., microelectrochemical cell). The rubber sheet also provides a good fluidic seal. The width of the microchannels is limited to 174 μm to prevent the microchannels from being clogged by the rubber sheet above after clamping the chip into the fixture. When the microchannel is wider than 190 μM, severe clogging is observed.

The Darcy-Weisbach equation [10] for the internal flow in ducts was used to calculate the pressure drop ΔP, assuming fully developed laminar flow through rectangular and circular ducts:

$$\Delta P = \rho f \frac{L}{D_h} \left(\frac{V^2}{2} \right) \quad (1)$$

where ρ is the density of electrolyte, f is the friction factor, L is the channel length, D_h is the hydraulic diameter, and V is the velocity of the electrolyte. The calculated pressure drop along the microfluidic channels and vertical through holes (2.1 mm diameter and 10.1 mm long) for 7.76 μL/s flow rate was 3.8 kPa. This flow rate is high enough to flush the entire flow channels and the electrochemical cell in 10 s. The pressure drop across the flow path is low enough to work with a commercial miniature peristaltic pump (e.g., P625, Instech Laboratories, Plymouth Meeting, PA, USA) for future analysis automation.

3. Results

3.1. Electrochemistry

The authors have previously published a detailed description of the electrochemistry of nitrate on silver in 1 M NaOH electrolyte

[8]. Cyclic-voltammetry (CV) on a silver disk electrode, which was made with a ground tip of 0.5 mm-diameter silver wire encapsulated in a plastic syringe, indicated that the electrochemical system showed high activity for nitrate reduction. A well-defined nitrate-reduction peak, separated from H_2O reduction was observed in the CV. The peak current was linear up to 50 mM, and a comparison of the sensitivity with CV results of other electrochemical systems showed that a silver electrode in NaOH electrolyte was sufficiently sensitive for amperometric nitrate determination.

With the electrochemistry established on the macroscopic scale, we worked to miniaturize the electrochemical cell. The electrodes in the microsensor are made of the same material but are produced in a thin-film form. The electrolyte for the microsensor was also NaOH, but a lower concentration was used, compared to 1 M NaOH used in the cyclic voltammetry of our previous study. The nitrate-reduction potential (i.e., −1.08 V) is very close to the hydroxide desorption potential (i.e., −1.0 V) [8]. As a result, hydroxide desorption contributes substantially to the background current, which ultimately increases the LOD. It is desirable to use a low-concentration electrolyte, because it was observed that the desorption peak decreased as the electrolyte concentration was reduced. However, the electrolyte concentration should be greater than the target nitrate concentration (i.e., at least 0.7 mM [2]), otherwise the electromigration of nitrate contributes significantly to the current detected, which would have the consequence of an analytical signal that is not linear with concentration. Also, a higher solution resistance could influence the sensing-electrode potential due to an uncompensated ohmic drop. Finally, a microfluidic channel formed in bare silicon by DRIE etching is attacked by highly concentrated hydroxide. Given the above considerations, a lower electrolyte concentration (i.e., 0.01 M) was used for the microsensor.

3.2. Electrochemical interference

The interference from 10 ions commonly found in groundwater (i.e., NO_2^-, Cl^-, HPO_4^{2-}/PO_4^{3-}, SO_4^{2-}, F^-, BO_2^-, $CO_3{}^{2-}$, K^+, Sr^{2+}, and Ca^{2+}) [11] was studied (note: phosphate ion in $Na_3PO_4 + 0.01$ M NaOH exists as approximately equal concentration of HPO_4^{2-} and $PO_4{}^{3-}$). Interference of the DPSC technique was quantified using a 0.5-mm-diameter silver disk electrode in two ways. First, a calibration curve (1 μM to 10 mM) for nitrate was obtained by DPSC. Then a 1000 μM solution of each ion was measured using the same analytical procedure, and the analytical signal was converted to equivalent nitrate concentration using the nitrate-calibration curves. This test informs us how much the proposed sensing scheme mistakenly measures nitrate when it is absent. The interference was negligible: less than 7 μM (equivalent nitrate) for most of the ions. This represents less than 1% of the allowable nitrate concentration. Even for NO_2^-, a major interfering ion in most nitrate analysis, interference was minimal (3.9 μM). Next, the 1000 μM nitrate was measured in the presence of 1000 μM of each interfering ion. This allows the effect of each interfering ion on the nitrate analytic signal to be determined. Fig. 4 is a bar graph illustrating the second interference effect. Interferences were also reasonably small (i.e., less than 10% signal distortion) except HPO_4^{2-}/PO_4^{3-}, Ca^{2+}, and Sr^{2+}, where the change in nitrate-equivalent concentration was more than 20% [8]. This result should be considered when real-world samples are analyzed.

3.3. Nitrate determination with the sensor chip

Sensor chips were tested for key performance parameters (i.e., LOD, linear range, and linearity). Nitrate concentrations were measured by connecting the electrical contacts on the sensor chip to the potentiostat (CHI-660B) and performing the DPSC process. Digitized current data was numerically integrated to calculate the nitrate reduction charge $Q_{NO_3^-}$.

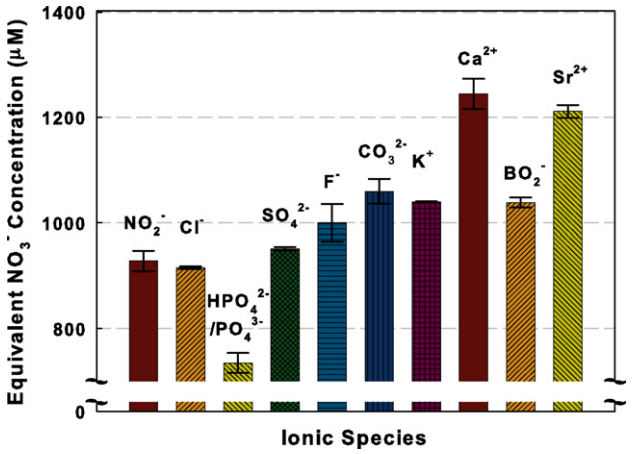

Fig. 4. Measured nitrate concentration in a 1000 μM nitrate solution when an ionic species of the same concentration is present.

Fig. 5 illustrates current output and chronocoulometric response of a sensor chip (chip #53) in 0.01 M NaOH. Vertical lines indi-

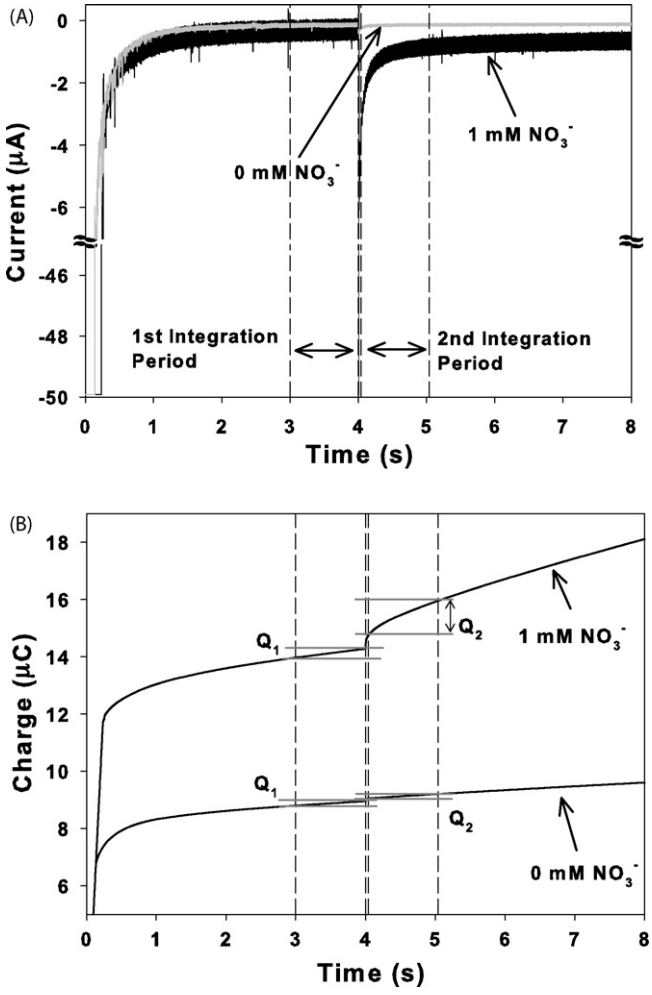

Fig. 5. (a) Current measured after applying double-potential steps to a sensor chip in blank electrolyte and 1 mM $NaNO_3$ + 0.01 M NaOH solution and (b) the chronocoulometric output obtained using DPSC technique.

cate the integration periods needed to calculate Q_1 and Q_2. As seen in Fig. 5a, the current output to the first potential step (i.e., OCPT $\rightarrow E_1$) for a blank electrolyte approached steady-state in 2 s. After the second potential step (i.e., $E_1 \rightarrow E_2$) was applied, the current increases, then returned to the original amplitude of E_1 in less than 2 s, because there was no nitrate present. A significant increase in current was observed when 1000 μM nitrate was present for the second potential step at E_2. One difference between our previous study [8] and this one is that spikes in the current output, which were much larger than random noise, were observed for the thin-film silver sensing electrode in 1000 μM nitrate solution. Inspection through a microscope revealed that silver was gradually lost as the DPSC repeated, and we speculate that such corrosion (i.e., rapid change in surface area) caused the current spikes.

Fig. 5b shows chronocoulometric signal for the blank electrolyte and nitrate solution. As opposed to the current output, charge grows as a function of time. Also, noise and spikes in the current output (Fig. 5a) are not observed in Fig. 5b, so uncertainty in measurement is reduced. This agrees with the SNR analysis of the previous study [8]. For the blank electrolyte, Q_1 and Q_2 are similar, so charge due to oxygen reduction is removed in $Q_{NO_3^-}$ by subtracting Q_1 from Q_2. Similarly, the oxygen background for the case where nitrate is present is also removed. The value of Q_2 for 1 mM nitrate solution grows much faster than one for the blank electrolyte, indicating increase of $Q_{NO_3^-}$ in proportion to nitrate concentration. The value of Q_1 for the nitrate solution is slightly bigger than the blank electrolyte although the same oxygen is reduced at E_1. This is because current due to random spikes are added to integration in addition to oxygen reduction current.

We speculate that evaporated thin-film silver is not electrochemically identical to the bulk silver used in silver wire (e.g., more susceptible to electrochemical corrosion). The fact that a severe potential drift was observed for the thin-film silver reference electrode when not anodized but such drift was not observed for macroscale silver wire, may support this argument. Regardless, the performance of the DPSC technique was not affected; calibration curves obtained using the thin-film silver ring electrode and the macroscopic silver disk electrode showed the similar characteristics (e.g., linearity, and linear range).

To examine sensor performance, successfully microfabricated chips were tested and calibration curves were obtained. In order to obtain calibration curves, $Q_{NO_3^-}$ was successively obtained with increasing nitrate concentration by the standard addition method (i.e., 1, 2, 5, 10, 20, 50, 100, 200, 500, and 1000 μM, and 2, 5, and 10 mM) using the DPSC technique. An on-chip silver-oxide reference electrode was used for all 6 chips. The reference potential of the thin-film silver-oxide electrode slowly drifts with time, and the potential lies between 0.188 and 0.215 V after oxide formation. The potential of a thin-film silver-oxide electrode was measured with a commercial Ag/AgCl reference electrode (i.e., RE-5B) before each experiment to ensure the proper reference potential.

A calibration curve is expressed as $y = a_0x + a_1$, where y represents the measured $Q_{NO_3^-}$, x is the concentration of nitrate standard, a_0 is the slope and a_1 is the intercept. The sensitivity S is given by to $S = a_0$ (unit: μM/C). The detection limit X_{DL} for analytic signal is defined as:

$$X_{DL} = \bar{X}_b + z\sigma_b \quad (2)$$

where $\bar{X}_b$ is the mean of $Q_{NO_3^-}$ at zero nitrate concentration, σ_b is the standard deviation, and z is the predetermined confidence level. LOD is expressed in concentration $C_{DL} = (X_{DL} - \bar{X}_b)/s$. C_{DL} is commonly calculated with predetermined confidence level $z = 3$ [12]. When calculating the LOD for sensor chips, it was not practical to obtain a true standard deviation σ_b in Eq. (2) because of the number of blank measurements had to be limited due to the relatively short electrode lifetime (15–25 measurements). We estimated σ_b with a sample standard deviation S_b and replaced z with a t-value from the *Student's-t* distribution, so that the detection limit was $X_{DL} = \bar{X}_b + tS_b$ [13]. S_b was calculated with $t = 2.776$ for a 97.5% confidence level and 4 degrees of freedom. The limit of detection in terms of concentration (C_{DL}) varied from die to die and ranged from 4 to 75 μM.

Fig. 6a shows the calibration curves of a chip (i.e., chip #41) that has a on-chip silver-oxide reference electrode. As observed in the previous silver-disk electrode experiments [8], the slope of the calibration curve for each of the chips was different over two concentration ranges. In this study, the linear range (i.e., the solid line) is defined from the LOD to the concentration at which the slope changes. (i.e., upper limit of linearity). For example, the linear range of chip #41 was from 42 μM to 2 mM. The chip was also linear from 2 to 10 mM, but with a different slope. The upper limit of linearity varied from chip to chip between 500 and 2000 μM. It was also noted that the calibration was sufficiently linear (i.e., R^2 is 0.99 in all the cases except for chip #11). Table 1 summarizes the measured parameters of the 6 chips. Fig. 6b shows statistical variation of $Q_{NO_3^-}$ at each concentration and a calibration curve that combines responses of all chips tested except chip #34. The averaged calibra-

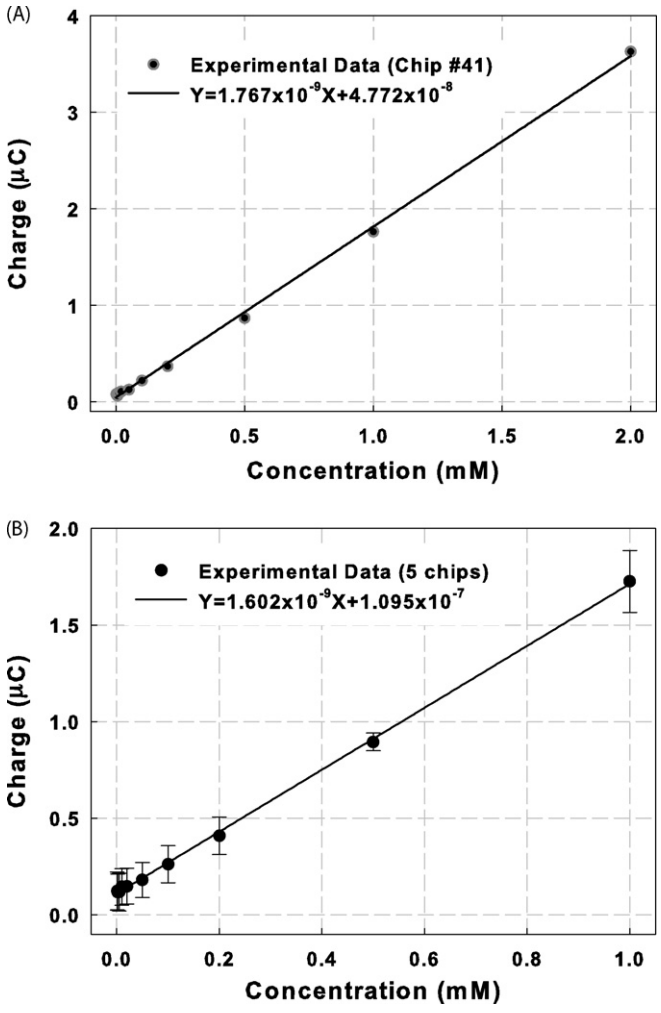

Fig. 6. Calibration curves for: (a) sensor chip #41 and (b) 5 sensor chips. All curves were obtained while using on-chip thin-film silver-oxide reference electrodes.

Table 1
Characterization of sensor chips tested with an on-chip silver-oxide reference electrode.

Chip	Calibration curves ($y =$)	Upper limit of linearity (μM)	LOD (μM)	Linearity (R^2)
11	$1.31 \times 10^{-9}x + 1.16 \times 10^{-8}$	1000	74.79	0.960
34	$5.30 \times 10^{-8}x - 3.07 \times 10^{-7}$	500	27.80	0.996
41	$1.77 \times 10^{-9}x + 4.77 \times 10^{-8}$	2000	46.64	0.999
53	$1.44 \times 10^{-9}x + 1.14 \times 10^{-8}$	500	18.08	0.996
55	$1.73 \times 10^{-9}x + 4.60 \times 10^{-7}$	2000	42.07	0.992
85	$1.66 \times 10^{-9}x + 2.26 \times 10^{-8}$	1000	3.96	0.997

tion was linear up to 1000 μM. From this figure, even though each chip responds differently at a given nitrate concentration, but the chip-to-chip variation is relatively small (i.e., $R^2 = 0.93$). As seen in Table 1, the sensitivity of chip #34 is 30 times greater than the other chips, and it is speculated that this is due to a manufacturing defect of the chip. One possible defect is that bad adhesion of polyimide protection layer results in the exposure of silver underneath the polyimide. During the microfabrication process, it was found that a major reason for low yield is bad adhesion of the polyimide layer. An exposed interconnect to the sensing electrode would result in an unexpectedly large surface area for the electrochemical reaction because the interconnect is also made of silver, which is the sensing electrode material.

The limited stability of thin-film electrodes was an issue in using these sensor chips. The sensing electrode degraded gradually because of the electrochemical activation process. We observed that when fast potential scans were applied as a part of the activation, the cyclic voltammogram shifted negatively or positively, little by little, as the number of cycles increased. We speculate that the shift observed in CV curves is due to a drift in the reference potential of the silver-oxide electrode. Scanning the potential either too negatively or too positively can create excessive oxidation or reduction of the thin-film silver sensing electrode, which ultimately damages the sensing electrode. Therefore, in order to study the effect of an unstable reference potential, 2 sensor chips (i.e, #12 and #76) were tested using the commercial Ag/AgCl reference electrode. The CV curves in the activation process looked normal without shift. It was observed that these 2 chips had better performance than the 6 chips tested with the thin-film silver-oxide reference electrode. The DPSC measurements of nitrate from 0 to 5 mM resulted in similar LODs but greater linear ranges (i.e., 12.57 μM to 5 mM for the chip #12 and 76.90 μM to 5 mM for the chip #76) as shown in Fig. 7. Also, a longer lifetime was observed for the 2 chips tested with a commercial macroscopic reference electrode, than for the 6 chips tested with the on-chip silver-oxide reference electrode. These 2 chips did not fail after 60 measurements. The linearity was as good as that observed with the other 6 chips tested with microscopic reference electrodes (i.e., $R^2 = 0.99$). Based on this comparison, we speculate that the performance of the sensor chip would be improved with a more stable reference electrode in terms of lifetime and linear range. In summary, the characterization of sensors tested with on-chip microscale silver-oxide reference electrodes is: (1) the LOD is 4–75 μM, (2) the upper limit of linearity is 500–2000 μM, and (3) the linearity is 0.99.

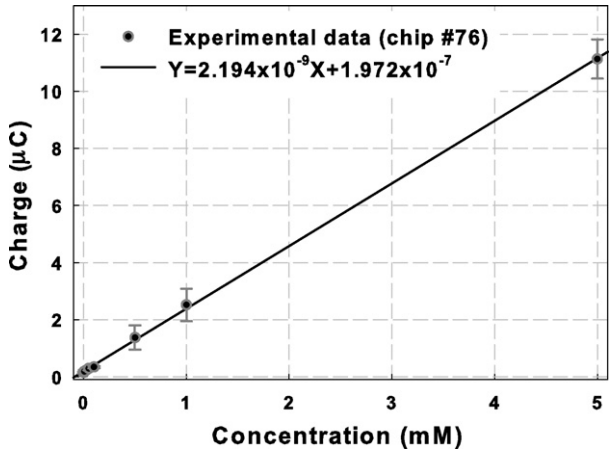

Fig. 7. A calibration curve for a nitrate-sensor chip tested with a commercial macroscopic Ag/AgCl reference electrode.

A sensor chip was also tested in the fixture (Fig. 3). The reference potential of the silver-oxide electrode was monitored before clamping the chip in the fixture. A 100-μM nitrate sample of was injected into the electrochemical cell of the fixture with a syringe. The measured analytic signal confirmed that the chip operated properly in a flow-through-type system.

4. Conclusions and discussion

A small-form-factor electrochemical nitrate sensor was microfabricated and thoroughly characterized by calibration curves generated with a DPSC technique in a simple electrochemical system (i.e., silver sensing electrode, sliver-oxide reference electrode, and platinum counter electrode in 0.01 M NaOH). Interference from ions commonly found in groundwater was minimal except for HPO_4^{2-}/PO_4^{3-}, Ca^{2+}, and Sr^{2+}. The prototype microfabricated sensor demonstrates the feasibility of using it for nitrate detection because of its low LOD (4–75 μM), broad linear range (2–3 orders of magnitude), and high linearity ($R^2 = 0.99$). The dynamic range can be extended to 4 orders of magnitude if the second linear portion of the calibration curves is also used. The custom-made fixture would allow the sensor to operate as a flow-through micro-analysis system because of its small cell volume (1.8 μL) and integrated microfluidic channels. The size of the sensor chip could be reduced so that the entire sensor could be smaller than those made here, because 73% of the area on the chip is not used. The analytical throughput will be relatively high because the DPSC process takes only about 2 min. A micropotentiostat [14] and low-power miniature pumps and valves could facilitate assembly of the nitrate-sensing system into a small package. Such a nitrate-sensing system could operate autonomously and wirelessly in sensor networks, if used with a wireless embedded-system platform. However, the limited stability of the sensor, which is primarily due to the unstable potential of the on-chip thin-film silver-oxide reference electrode, should be addressed. The thin-film sensing electrode could not survive the electrochemical activation process in the long term, because repetitive oxidation and reduction gradually dissolved the silver. An unstable potential will further exacerbate the silver-dissolution problem. A thick-film silver sensing electrode (e.g., electroplating or screen printing) could increase the lifetime. A possible solution to the unstable reference potential of silver-oxide electrode is to use a polymer-coated silver-chloride reference electrode, since we observed that a *polyurethane*-coated chloridized silver wire showed an improved stability (e.g., 3 mV drift in 27 h). A mercury–mercury oxide(II) reference electrode also could be a solution because of its stable potential in alkaline media [15]. Mercury has been integrated on microfabricated devices by electroplating, droplet generation by pressure, or manual pipetting. For example, mercury hemispheres were created by electroplating on metal electrodes for anodic stripping voltammetry [16]. For a Hg/HgO reference electrode HgO must be deposited on Hg, which is traditionally accomplished by adding a slurry of HgO powder and Hg. This HgO desposition could be challenging for mass microfabrication. In addition, containing a mercury

droplet stably at a fixed location would require very thick wall [17].

Acknowledgement

We would like to gratefully acknowledge that our research was funded by the NSF and Center for Embedded Network Sensing at UCLA (NSF CCR-0120778).

References

[1] C.S. Bruning-Fann, J.B. Kaneene, The effects of nitrate, nitrite, and N-nitroso compounds on human health: a review, Vet. Hum. Toxicol. 35 (1993) 237–253.
[2] Environmental Protection Agency, List of contaminants & their maximum contaminant level (MCLs), http://www.epa.gov/safewater/contaminants/dw_contamfs/nitrates.html.
[3] K.S. Johnson, J.A. Needoba, S.C. Riser, W.J. Showers, Chemical sensor networks for the aquatic environment, Chem. Rev. 107 (2007) 623–640.
[4] D. Diamond, S. Coyle, S. Scarmagnani, J. Hayes, Wireless sensor networks and chem-/biosensing, Chem. Rev. 108 (2008) 652–679.
[5] V. Majidi, C. Hassel, Miniaturized instrumentation for field applications: general considerations for environmental sensor networks, Int. J. Environ. Anal. Chem. 84 (2004) 1111–1121.
[6] M.J. Moorcroft, J. Davis, R.G. Compton, Detection and determination of nitrate and nitrite: a review, Talanta 54 (2001) 785–803.
[7] C.M.A. Brett, A.M.O. Brett, Electrochemistry: Principle, Methods, and Applications, Oxford University Press, New York, 1993, p. 206.
[8] D. Kim, I.B. Goldberg, J.W. Judy, Chronocoulometric determination of nitrate on silver electrode and sodium hydroxide, Analyst 132 (2007) 350–357.
[9] C.C. Liu, P.J. Hesketh, G.W. Hunter, Chemical microsensors, Interface 13 (2004) 22.
[10] M.C. Potter, D.C. Wiggert, Mechanics of Fluids, Prentice Hall, Englewood Cliffs, NJ, 1991, p. 250.
[11] S.N. Davis, R.J.M. DeWiest, Hydrogeology, John Wiley & Sons, New York, 1966, p. 111.
[12] H. Kaiser, Quantitation in elemental analysis, Anal. Chem. 42 (1970) 26A–59A.
[13] G.E.P. Box, W.G. Hunter, J.S. Hunter, Statistics for Experimenters, Wiley, New York, 1978, p. 49.
[14] A. Gore, S. Chakrabartty, S. Pal, E.C. Alocilja, Multichannel femtoampere-sensivity potentiostat array for biosensing applications, IEEE Trans. Circ. Sys. 53 (2006) 2357–2363.
[15] D.J.G. Ives, G.J. Janz, D.J.G. Ives, G.J. Janz, Reference Electrodes, Theory and Practice, Academic Press, New York, 1961, p. 335.
[16] G.T.A. Kovacs, C.W. Storment, S.P. Kounaves, Microfabricated heavy metal ion sensor, Sens. Actuators B: Chem 23 (1995) 41–47.
[17] X. Zhu, C. Gao, J. Choi, P. Bishop, C.H. Ahn, On-chip generated mercury microelectrode for heavy metal ion detection, Lab on a Chip 5 (2005) 212–217.

Biographies

Dohyun Kim received the B.S. degree in 1999, and the M.S. degree in 2001 from the department of mechanical engineering, Sogang University, Seoul, Korea. His research focus was modeling and designing of smart controller for CNC (Computer-Numerical-Control) machining centers. He is currently a doctoral candidate in electrical engineering department at University of California, Los Angeles. As a graduate student researcher, he has been developing a microfabricated electrochemical contaminant sensor for environmental sensor networks. His research interest includes chemical/biological electrochemical sensor and MEMS (micro electro mechanical system), and ion-exchange-membrane membrane-based miniaturized sample-preparation system.

Ira B. Goldberg received the Ph.D. degree from the University of Minnesota in 1969, and the B.A. degree from Adelphi University in 1964. He worked as a postdoctoral research fellow at the University of Texas from 1969 to 1971, and as principal scientist in materials science at the Rockwell Science Center from 1971 to 2002 where he worked on diverse problems in magnetic materials and measurements, magnetic resonance, microwave measurements and electrochemical/electrodeposition processes. He is currently a visiting scholar at the University of California at Los Angeles in the MEMS and Neuroengineering groups of Judylab where he is working on magnetic, and electroanalytical measurements. In addition he is teaching classes in physics and chemistry at California Lutheran University.

Jack W. Judy received the Ph.D. and M.S. degrees from the University of California, Berkeley, CA, in 1996 and 1994, respectively, as well as the B.S.E.E. degree, with summa cum laude honors, from the University of Minnesota, Minneapolis, MN, in 1989. He has been on the faculty of the electrical engineering department at the University of California, Los Angeles, since 1997, where he is currently an associate professor. He has also worked for Silicon Light Machines, Inc., Sunnyvale, CA, an optical-MEMS startup company, from 1996 to 1997. In his doctoral research he developed a novel ferromagnetic microactuator technology that is useful for a variety of applications, including optical, RF, and biological MEMS. At UCLA he is the Director of the Nanoelectronics Research Facility, the Director of the Microfabrication Instructional Laboratory, and the Chair of the MEMS and Nanotechnology Major Field of the Electrical Engineering Department. Dr. Judy also Co-Founded and Directs the UCLA NeuroEngineering Training Program, which is sponsored jointly by the Biomedical Engineering and Neuroscience Interdepartmental Programs and is the first found NeuroEngineering training program in the world. His present research interests include additional novel ferromagnetic MEMS and NEMS, wireless chemical sensors, micromachined sensors for plasma research, novel 3D micromachining techniques and a variety of neuroengineering projects, such as high-density microelectrode arrays for interfacing to the retina and other biological tissues, dynamic simulation of 3D neural–electronic interfaces, micromachined multielectrode neural probes, wireless neural transceivers, brain–computer interfaces, deep brain stimulation, mapping and activating locomotion in spinal cord injury, and restoring ocular motility.